10-1-2008

Pulsar timing as a probe of non-einsteinlan polarizations of gravitational waves

K. J. Lee

F. A. Jenet

Richard H. Price

Recommended Citation

K. J. Lee, et. al., (2008) Pulsar timing as a probe of non-einsteinlan polarizations of gravitational waves.Astrophysical Journal685:21304. DOI: http://doi.org/10.1086/591080

The Astrophysical Journal, 685:1304–1319, 2008 October 1

PULSAR TIMING AS A PROBE OF NON-EINSTEINIAN POLARIZATIONS OF GRAVITATIONAL WAVES

K. J. Lee,[1,2] F. A. Jenet,[1] and Richard H. Price[1]

Received 2008 May 23; accepted 2008 June 14

ABSTRACT

Einstein's theory of gravity predicts waves of the distortion of spacetime with two degrees of polarization; alternative theories predict more polarizations, up to a maximum of six. Although laser interferometric gravity wave detectors can be used to search for at least some of the non-Einsteinian polarizations, their configuration is not optimal for the task. By contrast, the angular distribution of pulsars in the sky makes pulsar timing a flexible tool for detecting all polarizations. We give here an analysis of the sensitivity of pulsar timing to an isotropic stochastic gravitational wave background of waves with non-Einsteinian polarizations and conclude that their detection may be feasible in the near future. In particular, we compute the number of pulsars necessary to detect a stochastic background made up of one type of polarization and to distinguish non-Einsteinian from standard polarizations. We conclude that for biweekly observations made for five years with rms timing accuracy of 100 ns, detecting non-Einsteinian modes will require: 60 pulsars in the case of the longitudinal mode; 60 for the two spin-1 "shear" modes; and 40 for the spin-0 "breathing" mode. These are targets that should be easily achievable with the proposed Square Kilometer Array project. To discriminate non-Einsteinian modes from Einsteinian modes, we need 40 pulsars for the breathing mode, 100 pulsars for the longitudinal mode, and 500 pulsars for the shear mode. We confirm the previous estimate that 40 pulsars are needed to detect the spin-2 "transverse" (Einsteinian) polarizations. Better focused statistical tests may allow improvements in sensitivity for some of these polarizations.

Subject headings: gravitational waves — pulsars: general

1. INTRODUCTION

Einstein's general theory of relativity has been extremely successful in describing gravitational physics, but there remain many feasible alternative gravity theories (Will 2006). Interest in such theories has increased recently due to discoveries in galactic dynamics and cosmology, i.e., dark matter and cosmic acceleration (see the review Sanders & McGaugh 2002). Experiments have shown that almost all gravitational theories must be metric theories (Will 2006). In such theories, gravitational waves (GWs) can have up to six possible polarization states, four more than are allowed by general relativity (GR), Einstein's theory. Hence, in principle, GR can be tested by measuring the polarization properties of GWs (Eardley et al. 1973).

Analysis of pulse time-of-arrival (TOA) data shows that pulsars, especially millisecond pulsars, are very stable clocks. Measurement of timing residuals, that is, the differences between observed and predicted TOAs, enables the direct detection of GWs (Estabrook & Wahlquist 1975; Sazhin 1978; Detweiler 1979). If fluctuations of TOAs are induced by GWs, there will be correlations of the fluctuations between widely spaced pulsars. Hellings & Downs (1983) attempted to detect this effect by cross-correlating the time derivative of the timing residuals of multiple pulsars. Jenet et al. (2005) took an approach based directly on the residuals, rather than on their time derivative. Their technique uses multiple pulsar observations to make an unambiguous detection of an isotropic stochastic GW background. All of the above work considered only the GWs of Einstein's theory.

In the current paper we extend the work of Jenet et al. (2005) to include the other four possible GW modes present in a general metric theory. As in the previous work, we assume an isotropic, stochastic GW background. Such a background of GWs will induce correlations between the timing residuals of any two pulsars. The GW-induced correlation of the TOAs of the two pulsars, $C(\theta)$, will depend on the angular separation θ between the pulsars. It is shown here that the exact functional form of $C(\theta)$ depends on the polarization states of the GW stochastic background. The θ-dependence of the measured correlation function, therefore, may be used to determine the polarizations possessed by the GWs inducing the fluctuations.

Unlike bar or interferometric detection, the detection of GWs based on radio pulsars includes a large number ($\geq$20) of spacetime probes or "arms." This greater directional complexity seems to make it superior for detecting and distinguishing modes of GW polarization. Unfortunately, at present it is difficult to compare the pulsar timing technique to those of bar and interferometer detectors, since little work has been done to determine the effectiveness of those detectors for detecting the full six polarization modes.

This paper is organized as follows. The correlation functions for a stochastic background of GWs are calculated in § 2, for each of the six possible polarization states, with further details given in Appendix A. In § 3, these correlation functions are used to determine how well a GW background of each polarization type could be detected and how the detectability depends on the number of pulsars used, the duration of observations of these pulsars, and the timing accuracy of their TOAs. An algorithm to discriminate the non-Einsteinian modes from GR modes is presented in § 4. This algorithm is used to find the minimum amplitude of a non-Einsteinian mode if that mode is to be detected with a given number of pulsars, for a given intrinsic noise level and a given power in a background of Einsteinian modes. A discussion of the results of this paper is given in § 5.

2. PULSAR RESIDUAL CORRELATION FUNCTIONS

The GW-induced correlation functions between timing residuals of two pulsars are calculated here for all six possible polarizations. As described in detail in Appendix A, the polarizations can be divided into two classes. For the purely transverse polarizations,

[1] CGWA, University of Texas at Brownsville, Brownsville, TX 78520; kjlee007@gmail.com.
[2] Department of Astronomy, Peking University, Beijing, 100871, China.

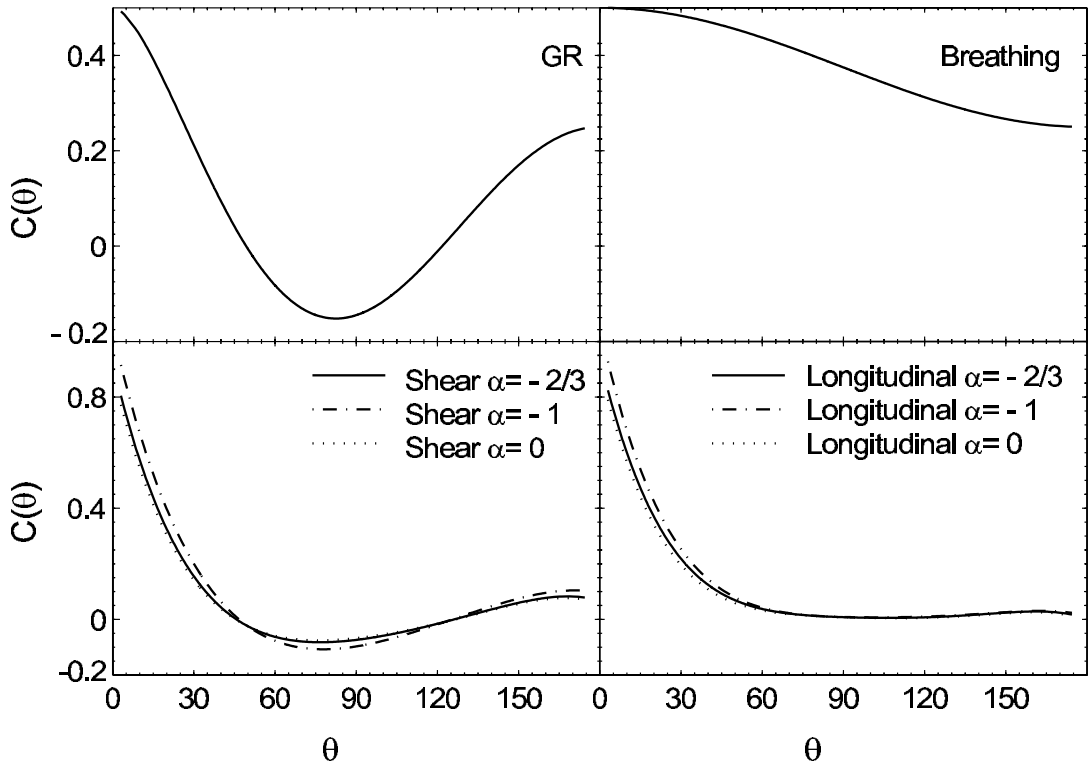

FIG. 1.—Normalized pulsar timing residual correlation coefficient, $\zeta^P = C^P(\theta)/C^P(0)$. Here, θ is the angular separation between two pulsars. "GR" stands for the two transverse traceless modes, "+" and "×." For the shear and longitudinal modes, the plots are the curves fitted with the expansion coefficients in Table 1, for five years of observation. Results are given for several values of α, the power-law index of the GW spectrum. The change in $\zeta^{\mathrm{sn,se},l}$ is on the order of 10^{-2} for a change in α from 0 to −1.

the GR and breathing modes, the GW-induced correlation functions can be calculated analytically. For the shear and longitudinal polarizations, modes that are not purely transverse, the correlation function must be computed with Monte Carlo simulations.

We consider a distribution of plane GWs in a general metric theory of gravity. The function $h^P(f,\hat{\boldsymbol{e}}_z)df\,d\Omega$ denotes the distribution of GWs of polarization P, in the frequency interval df and in the solid angle $d\Omega$ around the propagation direction $\hat{\boldsymbol{e}}_z$, such that the GW metric perturbation, at a given spacetime point $(t,\boldsymbol{r})$ is

$$h_{ab}(t,\boldsymbol{r}) = \sum_{P=+,\times,b,\mathrm{sn,se},l} \int_{-\infty}^{\infty} df \int d\Omega\, h^P(f,\hat{\boldsymbol{e}}_z) e^{2\pi i f(t-\boldsymbol{r}\cdot\hat{\boldsymbol{e}}_z/c)} P_{ab}(\hat{\boldsymbol{e}}_z). \quad (1)$$

The polarization index P indicates any of the polarization states $+$, $\times$, b, sn, se, and l; the "+" and "×" denote the two different GR spin-2 transverse traceless polarization modes; the "sn" and "se" denote the two spin-1 shear modes; the "l" and "b" denote the spin-0 longitudinal mode and the spin-0 breathing mode, respectively.

In this paper, we apply equation (1) to a stochastic background of GWs. This stochastic background is a superposition of monochromatic plane wave components with a frequency chosen at random from a predetermined spectrum, for our purposes always a power-law spectrum. The propagation direction of each plane wave component is chosen at random from an isotropic distribution. For a given plane wave component, the polarization tensor ϵ^P_{ab} for the polarization state P depends on the direction of propagation (e.g., it is parallel to the propagation direction for the

TABLE 1

EXPANSION COEFFICIENTS OF THE NORMALIZED CROSS-CORRELATION FUNCTION, $\zeta(\theta) = C(\theta)/C(0)$

α	c_0	c_1	c_2	c_3	c_4	c_5
			c_k for $C^{\mathrm{sn,se}}(\theta)$			
0	0.0378	−0.0871	0.1928	−0.1086	0.0239	−0.0073
−2/3	0.0317	−0.0739	0.1603	−0.0955	0.0289	−0.0121
−1	0.0298	−0.0700	0.1511	−0.0917	0.0302	−0.0135
			c_k for $C^l(\theta)$			
0	0.0584	−0.1206	0.1386	−0.0908	0.0409	−0.0147
−2/3	0.0512	−0.1057	0.1220	−0.0805	0.0373	−0.0156
−1	0.0470	−0.0987	0.1148	−0.0785	0.0388	−0.0175

NOTES.—We obtain this table using Legendre polynomials, i.e., $\zeta(\theta) = \sum_{k=0}^{N} c_k P_k(2\theta/\pi - 1)$ with $0 \le \theta \le \pi$. Note that these expansions are not applicable when $\theta = 0$. The α column indicates the power index of the GW background. By using these normalized cross-correlation functions, $\zeta(\theta)$, and by calculating $C(0)$ from eq. (A37), the cross-correlation functions $C(\theta)$ can be found.

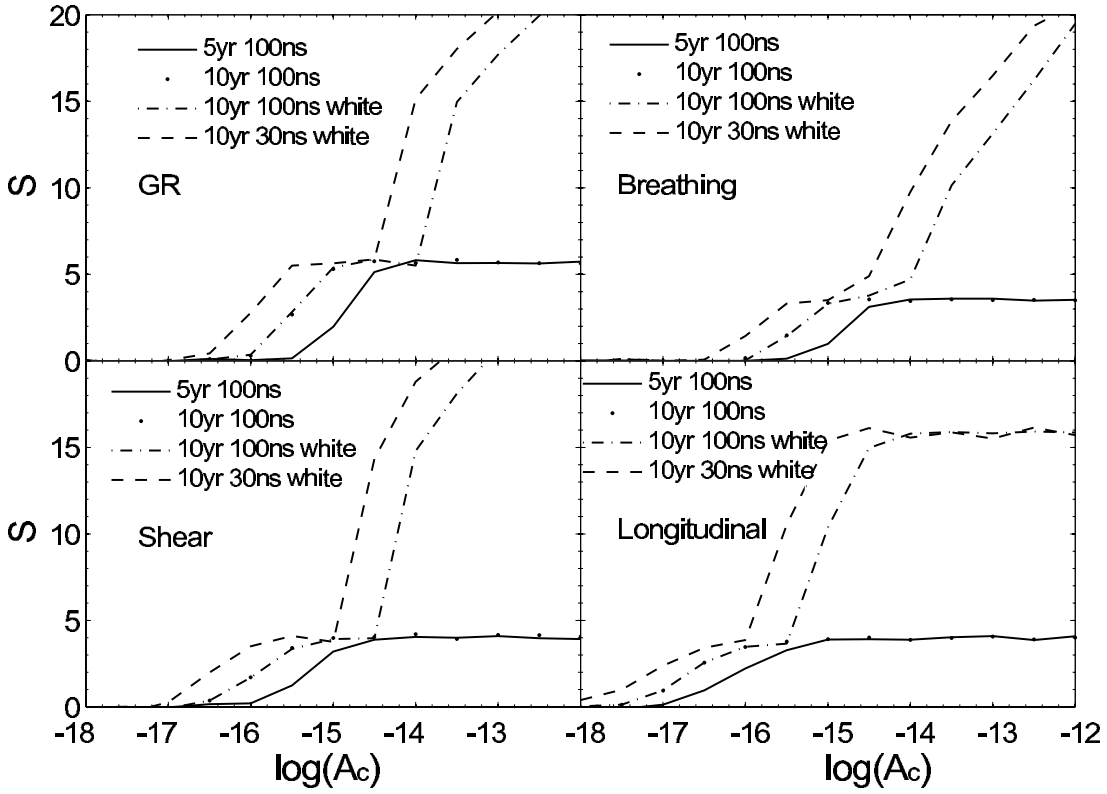

FIG. 2.—Detectability statistic S, as a function of A_c, for GWs with different polarization states, different durations of observation, and different levels of pulsar timing noise. Curve labels are the same as those of Fig. 1. The 100 ns and 30 ns labels indicate the level of intrinsic pulsar timing noise. The note "white" indicates the inclusion of the whitening technique described in the text. For the GR and breathing modes, 40 pulsars are used in the simulation; for the shear and longitudinal modes, 60 pulsars are used. The average Earth-pulsar distance is assumed to be 3 kpc, with a variance for the distance distribution of 0.6 kpc.

longitudinal mode). For some of the determinations we choose the stochastic background to be in a pure polarization state: Einsteinian, longitudinal, shear, or breathing. For the Einsteinian and shear modes (which have two states each), the plane of polarization of each component is chosen independently of the plane for any other component. In the case that we mix non-Einsteinian modes with a background of Einsteinian modes, the polarization of each component is chosen independently, subject only to a predetermined ratio of power in the Einsteinian and non-Einsteinian polarizations.

The frequency shift, $\Delta\omega/\omega$, of a pulsar timing signal induced by a plane GW traveling in the $\hat{\boldsymbol{e}}_z$-direction is (Detweiler 1979)

$$\frac{\Delta\omega}{\omega} = \frac{1}{2}(1 + \hat{\boldsymbol{e}}_z \cdot \hat{\boldsymbol{n}})^{-1}\hat{\boldsymbol{n}}_a\hat{\boldsymbol{n}}_b\left[h_{ab}(t,0) - h_{ab}\left(t - \frac{|\boldsymbol{r}_{\rm pul}|}{c}, |\boldsymbol{r}_{\rm pul}|\right)\right], \quad (2)$$

where it is assumed that the observer is located at $\boldsymbol{r} = 0$ and $\hat{\boldsymbol{n}}$ is the unit vector pointing from the observer to the pulsar. Both Sazhin (1978) and Detweiler (1979) showed that the above result is valid for the Einsteinian modes. It has been shown that this result holds for the other four modes as well (see Jenet et al. 2008, in preparation). Note that the denominator factor $(1 + \hat{\boldsymbol{e}}_z \cdot \hat{\boldsymbol{n}})$, in equation (2), vanishes for a GW wave propagating parallel to the pulsar signal. It is this denominator that underlies the very different sort of calculation needed for the angular correlations of the modes that are purely transverse and those that are not.

The frequency shift in equation (2) produces a GW-induced pulsar timing residual

$$R(t) = \int_0^t \frac{\Delta\omega}{\omega}(\tau)d\tau \quad (3)$$

that depends on the angular position of the pulsar. For two pulsars i and j separated by angle θ, we denote the cross-correlation function of the timing signal as $C(\theta) = \langle(R_i(t)R_j(t)\rangle$, where the angle brackets stand for the ensemble average over a stochastic GW background. For a mixture of polarizations, if the polarizations and the planes of polarization for each plane wave are chosen independently, as in our stochastic background, then $C(\theta)$ can be decomposed into six independent parts (see Appendix A for details). Each of these parts is induced by only one specific polarization mode, i.e., $C(\theta) = \sum_P C^P(\theta)$, with P ranging over $+$, $\times$, b, sn, se, and l.

For the Einsteinian modes and for the breathing mode, the cross-correlation function $C^P(\theta)$ is independent of Earth-pulsar

TABLE 2
EXPECTED PARAMETERS FOR PREDICTED STOCHASTIC BACKGROUNDS

Model	A_c	α	References
Supermassive black holes.....	10^{-15} to 10^{-14}	$-2/3$	1, 2, 3
Relic GWs.....	10^{-17} to 10^{-15}	-1 to -0.8	4
Cosmic string.....	10^{-16} to 10^{-14}	$-7/6$	5

REFERENCES.—(1) Jaffe & Backer 2003; (2) Wyithe & Loeb 2003; (3) Enoki et al. 2004; (4) Grishchuk 2005; (5) Maggiore 2000.

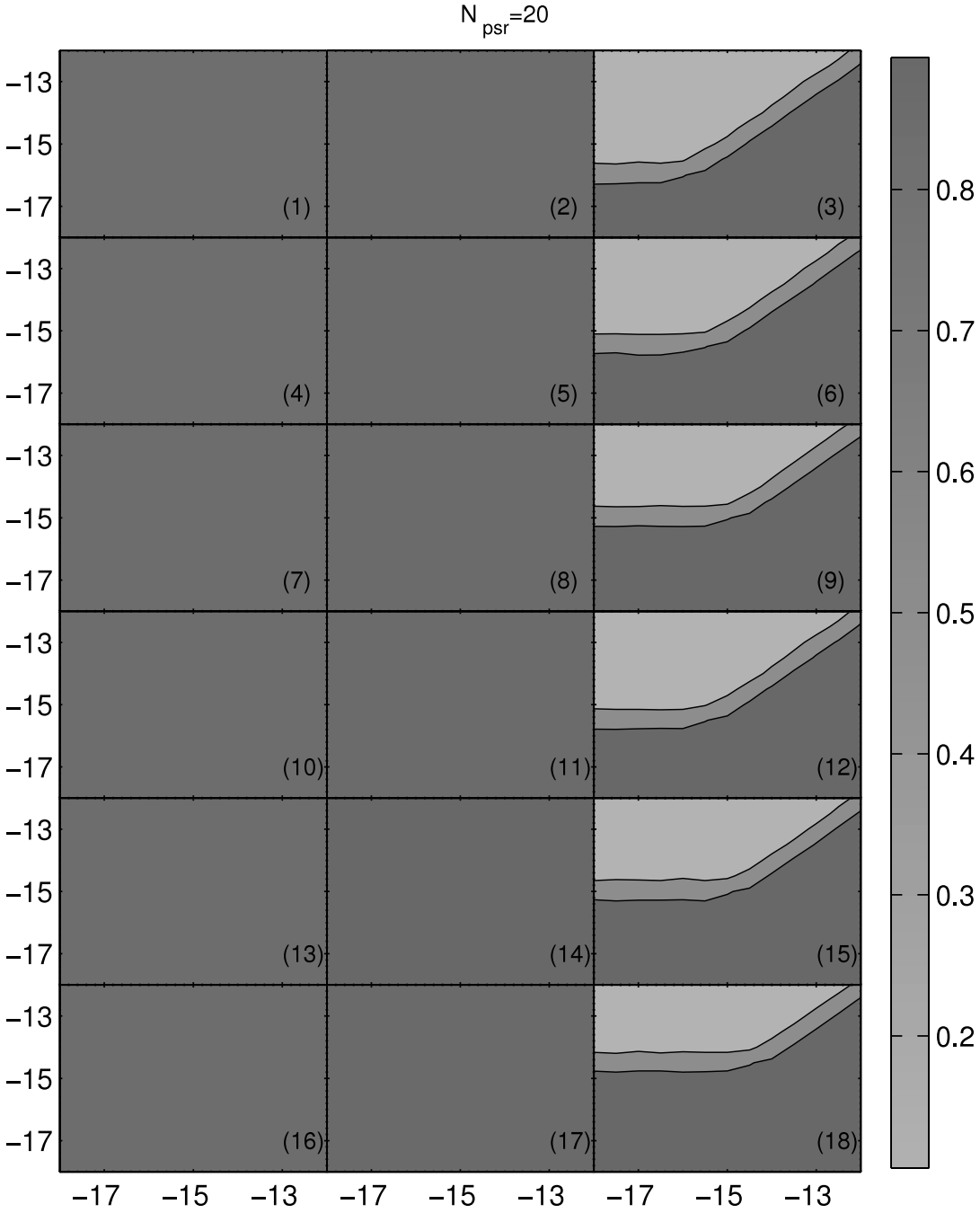

FIG. 3.—Contours of 10%, 50%, and 90% false dismissal rates for detecting a non-Einsteinian mode in the presence of a background of Einsteinian GWs. The white region (shown in subsequent figures) is 10% false dismissal rate; the darkest gray (two leftmost columns of this figure) indicates more than 90% false dismissal. It is assumed that the false alarm rate is 0.001, that the power index of the GWs is $-2/3$, and that 20 pulsars are used. The axes give the base 10 logarithm of the characteristic strains: the horizontal axis for the Einsteinian mode and the vertical axis for one of the non-Einsteinian modes. Each panel is labeled by a number at the bottom right corner; the corresponding parameters (noise level, duration of observation, polarization type) for each panel are given in Table 3. The panels are organized so that the left column shows results for shear modes, the middle for longitudinal modes, and the right for breathing modes.

distances and independent of the GW characteristic strain spectrum. (The precise definition of the characteristic strain is given in Appendix A.) General analytic forms for these correlation functions can therefore be derived. (See eqs. [A30] and [A33] in Appendix A.) In contrast, for the modes that are not purely transverse, the shear and longitudinal modes, the cross-correlation functions depend on the specifics of the strain spectra and on the pulsar distribution in distance. Since the duration of observation determines the lowest observable frequency, it turns out that the $C^{\mathrm{sn,se},l}(\theta)$ are also observation-span dependent. We used Monte Carlo techniques to calculate the $C^{\mathrm{sn,se},l}(\theta)$ for a power-law GW background and a representative sample of pulsars. For each polarization mode, the corresponding characteristic strain spectrum (defined in eq. [A1] of Appendix A) is assumed to be of the form $h_c^P(f) = A_c^P(f/f_c)^\alpha$, where α is the power-law index of the GW background.

In our Monte Carlo simulation, we choose and hold fixed a representative sample of pulsars and, thereby, fix the set of angles θ separating pairs of pulsars. We next generate a stochastic set of 10^4 GW wave sources, each with a specific polarization state P that is fixed for each simulation. Then the GW-induced TOA fluctuations for all the pulsars are calculated (see eq. [A8] of Appendix A), and the correlation function $C^P(\theta)$ is computed.

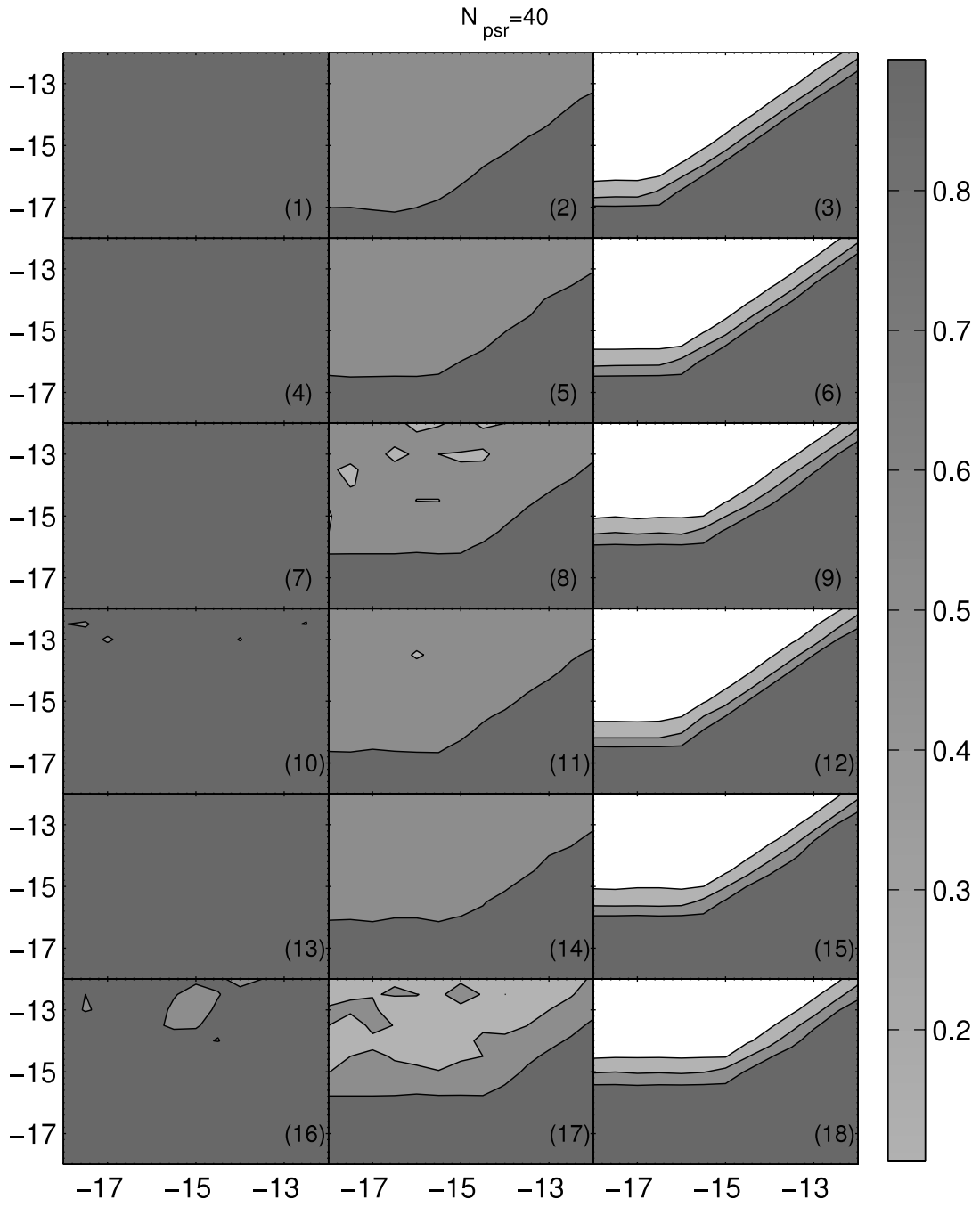

FIG. 4.— Same as Fig. 3, but for 40 pulsars.

A new stochastic GW background is then generated, and the computation of $C^P(\theta)$ is repeated. The computations of $C^P(\theta)$ are averaged together, and the process is repeated until the change in the average $C^P(\theta)$ is less than 0.1% for each value of θ in the pulsar sample. In Figure 1 we give the results of this process for the normalized cross-correlation function

$$\zeta^P(\theta) = C^P(\theta)/C^P(0), \tag{4}$$

for the purely transverse modes $P = +, \times$, and b.

As explained in § 1, the $C^P(\theta)$ for the sn, se, and l modes depend on the GW spectrum, so results must be given for a range of values of the power-law index α. In principle, the results are also sensitive to the time span of observations. We have found, however, that results are the same, up to absolute changes of 10^{-2}, for all observationally relevant time spans (years to tens of years). These results are given in Table 1, which presents coefficients for expanding normalized cross-correlation functions $\zeta(\theta)$ for the shear and longitudinal modes in Legendre polynomials. These curves are plotted, along with the Einsteinian and breathing mode curves, in Figure 1. Since the autocorrelation $C^P(0)$ is discontinuously large, it has been omitted from the curve fitting and from Figure 1.

3. ESTIMATING THE DETECTABILITY OF A GIVEN POLARIZATION MODE

As shown in Figure 1, the cross-correlation between two pulsar timing signals is a function of the angular separation θ between

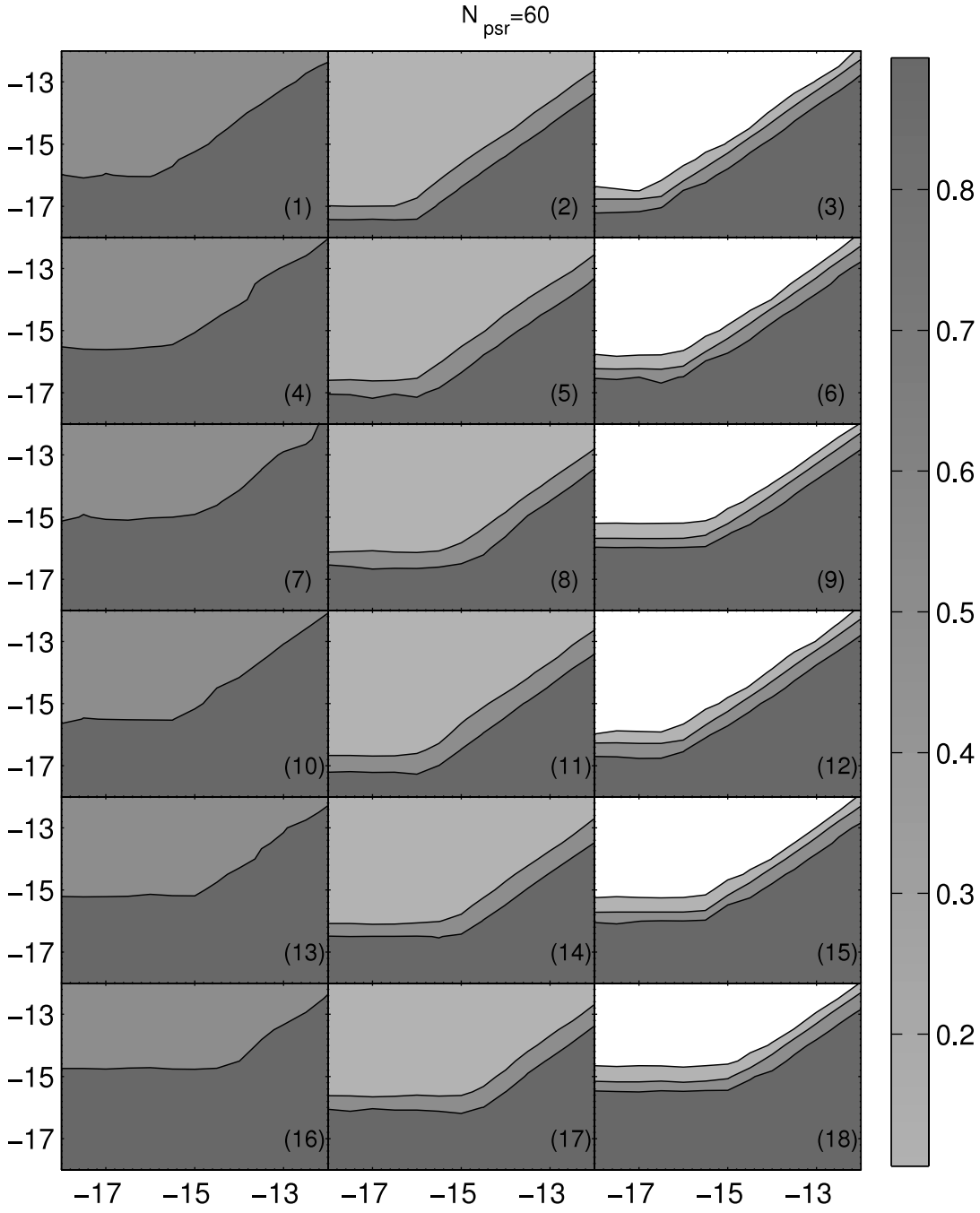

FIG. 5.—Same as Fig. 3, but for 60 pulsars.

pulsars, and the shape of the $C^P(\theta)$ curve strongly depends on the polarization properties of the GW backgrounds. Thanks to this polarization dependence, the polarization properties of the GWs can be detected through comparison of the theoretical (i.e., computed) correlation functions $C^P(\theta)$, for each polarization mode, with the observed correlations $c(\theta_j)$ defined by

$$c(\theta_j) = \frac{\sum_{i=0}^{N-1} \left[R_a(t_i) - \overline{R_a(t_i)}\right]\left[R_b(t_i) - \overline{R_b(t_i)}\right]}{\sqrt{\sum_{i=0}^{N-1} \left[R_a(t_i) - \overline{R_a(t_i)}\right]^2 \sum_{i=0}^{N-1} \left[R_b(t_i) - \overline{R_b(t_i)}\right]^2}}, \tag{5}$$

where $R_a(t_i)$ and $R_b(t_i)$ are the timing residuals of pulsar "a" and "b" at time t_i and where N is the number of observations. Here, θ_j is the angle between the direction pointing to the pulsar "a" and the direction pointing to the pulsar "b." The index j runs from 1 to the number of pulsar pairs $M = (N_p - 1)N_p/2$, because the autocorrelations are not taken into account.

Following Jenet et al. (2005) we next define

$$\rho = \frac{\sum_{j=1}^{M} \left[C(\theta_j) - \overline{C}\right]\left[c(\theta_j) - \overline{c}\right]}{\sqrt{\sum_{j=1}^{M} \left[C(\theta_j) - \overline{C}\right]^2 \sum_{j=1}^{M} \left[c(\theta_j) - \overline{c}\right]^2}}, \tag{6}$$

where $\overline{C} = \sum_{i=1}^{M} C(\theta_i)/M$ and $\overline{c} = \sum_{i=1}^{M} c(\theta_i)/M$. Then the statistic S describing the significance of the detection of a given polarization mode is $S = M^{1/2}\rho$. This statistic can be used to judge whether the observed correlations are more than random.

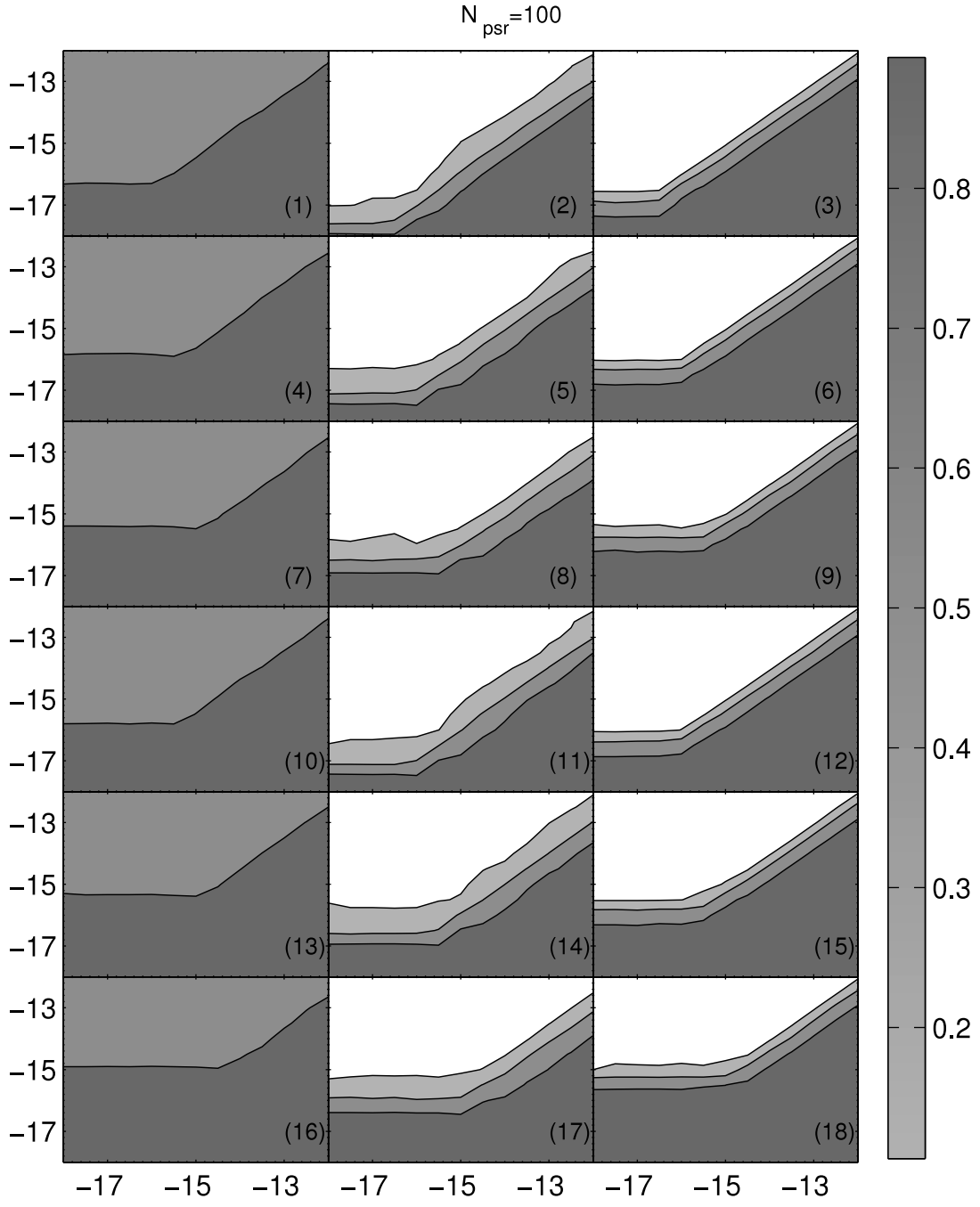

FIG. 6.— Same as Fig. 3, but for 100 pulsars.

In particular, we consider the case in which each $c(\theta_j)$ is chosen randomly from a Gaussian distribution and is chosen independently from $c(\theta_i)$ with $i \neq j$. In this case, the probability of getting a detection significance larger than S is $\mathrm{erfc}(S/\sqrt{2})/2$.

Our goal is to determine what will be needed in order to detect non-Einsteinian polarizations. To do this we need to find an expected value of S for each observational scenario considered, i.e., for each set of observational parameters: the number and distances of pulsars in the study; the duration and frequency of observation; the accuracy with which residuals can be timed; and the amplitude and spectral index α of the GW stochastic background. To get the expected S we use a second Monte Carlo simulation, distinct from the Monte Carlo simulation, described earlier, that was used to determine the values of the "theoretical" correlation functions $C(\theta)$. This second Monte Carlo simulation uses two main steps.

For a fixed pulsar sample, the first step is to calculate the theoretical $C^P(\theta)$ for a given polarization, duration of observation, and GW spectrum as outlined in § 2 and detailed in Appendix A. The second step consists of the following recipe:

1. Generate a large number ($\sim 10^3$) of monochromatic GW sources, such that the total GW background gives the expected power spectrum. Record the location, amplitude, phase, and polarization mode of each source.

2. Calculate the timing signal for all the pulsars by using equations (2) and (3).

3. Add white Gaussian noise to each pulsar's timing data to model the effects of non-GW noise processes.

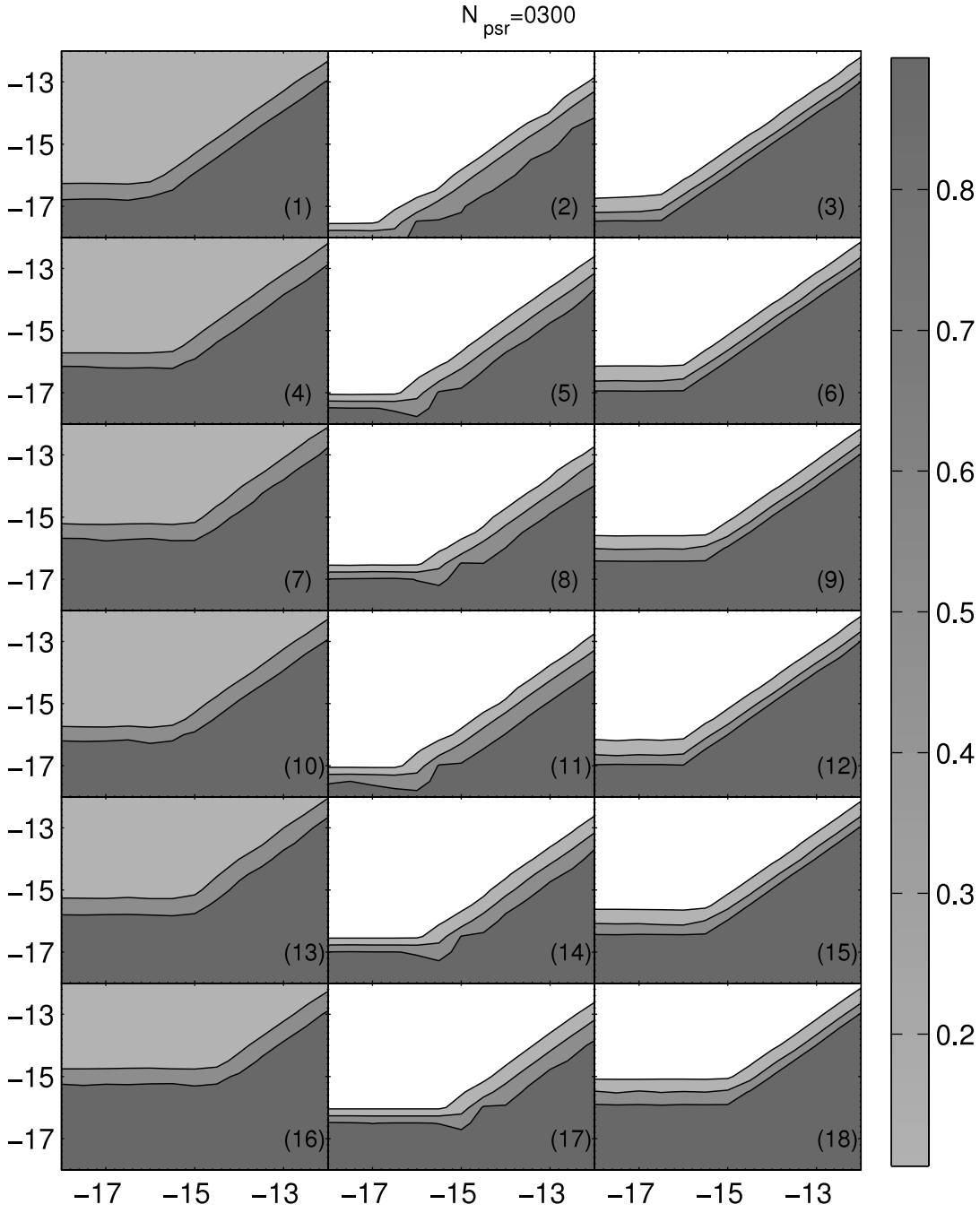

FIG. 7.—Same as Fig. 3, but for 300 pulsars.

4. Calculate the observational correlation coefficient $c(\theta_j)$ between pulsar pairs according to equation (5).

5. Calculate S from equation (6).

Repeat the steps above until the expected value of S converges.

The resulting detectability statistic S, for different GW polarization modes, is given in Figure 2. That figure includes the results of applying the whitening procedure of Jenet et al. (2005). The whitened curves dramatically illustrate the improvement in S in the case of strong GW signals (large GW amplitude factor A_c).

Note that here, and in the computations of § 4, the sample of pulsars is held fixed during the sequence of Monte Carlo simulations, and that for a given number (say 40) of pulsars, the same pulsar sample is used to compute both the "theoretical" $C^P(\theta)$ and the "measured" $c(\theta)$. In principle, conclusions about the S statistic could be sensitive to the details of the particular pulsar sample. We have checked this sensitivity by recomputing with a different set of pulsars (e.g., replacing a set of 40 pulsars by a different set of 40) and have found only insignificant differences in the values of S.

4. DISCRIMINATING NON-EINSTEINIAN MODES FROM THE EINSTEINIAN MODES

In contrast with § 3, in which each GW mode is considered independently, this section develops the necessary techniques to discriminate the non-Einsteinian modes from the Einsteinian modes and estimates the minimum detectable amplitude of a non-Einsteinian mode when a background of Einsteinian GWs is present.

TABLE 3
PARAMETERS FOR THE FALSE DISMISSAL RATE CONTOURS OF FIGURES 3–7

Number	σ_n	$N_{\rm obs}$	Mode
1	30	512	S
2	30	512	L
3	30	512	B
4	30	256	S
5	30	256	L
6	30	256	B
7	30	128	S
8	30	128	L
9	30	128	B
10	100	512	S
11	100	512	L
12	100	512	B
13	100	256	S
14	100	256	L
15	100	256	B
16	100	128	S
17	100	128	L
18	100	128	B

NOTES.—Here, σ_n is the averaged pulsar intrinsic noise level, and $N_{\rm obs}$ is the observing duration in units of weeks; the capital letters "S," "L," and "B" indicate, respectively, the case of shear and GR modes, longitudinal and GR modes, and breathing and GR modes. Each row in this table corresponds to a panel in Figs. 3–7 with the same index number that is given in the first column.

In general, the theoretical GW-induced correlation $C(\theta)$ is a sum of the theoretical correlations induced by each individual mode,

$$C(\theta) = \sum_P C^P(\theta) = \sum_P C^P(0)\zeta^P(\theta), \tag{7}$$

where $C^P(0)$ plays the role of an amplitude of excitation of mode P. Let $c(\theta)$ be the measured cross-correlation function normalized so that $c(0) = 1$. Its expected value, $\langle c(\theta)\rangle$, takes the form

$$\langle c(\theta)\rangle = \frac{\sum_P C^P(0)\zeta^P(\theta) + \sigma_n^2\delta(\theta)}{\sum_P C^P(0) + \sigma_n^2}, \tag{8}$$

where $\delta(0) = 1$ and $\delta(\theta) = 0$ for $\theta \neq 0$. We assume that the non-GW-induced timing fluctuations are described by a white Gaussian noise process with a variance given by σ_n^2. The ratio $\gamma^P = C^P(0)/\sigma_n^2$ is an indicator of the presence of a "P" mode GW. In terms of this ratio we can write the measured cross-correlation as

$$\langle c(\theta)\rangle = \frac{\sum_P \gamma^P\zeta^P(\theta) + \delta(\theta)}{\sum_P \gamma^P + 1}. \tag{9}$$

In searching for GW signals, we use the above form for $\langle c(\theta)\rangle$ to determine the values of the unknown parameters γ^P from data $c(\theta_i)$ by using a least-squares-type method. This is done with the following "cost function" calculated from the measured data,

$$K(\gamma^P) = \begin{cases} \sum_{i=0}^{M}\left(\dfrac{\sum_P \gamma^P\zeta^P(\theta_i) + \delta(\theta_i)}{\sum_P \gamma^P + 1} - c(\theta_i)\right)^2, & \text{if all of the } \gamma^P \geq 0, \\ M, & \text{if any of the } \gamma^P < 0, \end{cases} \tag{10}$$

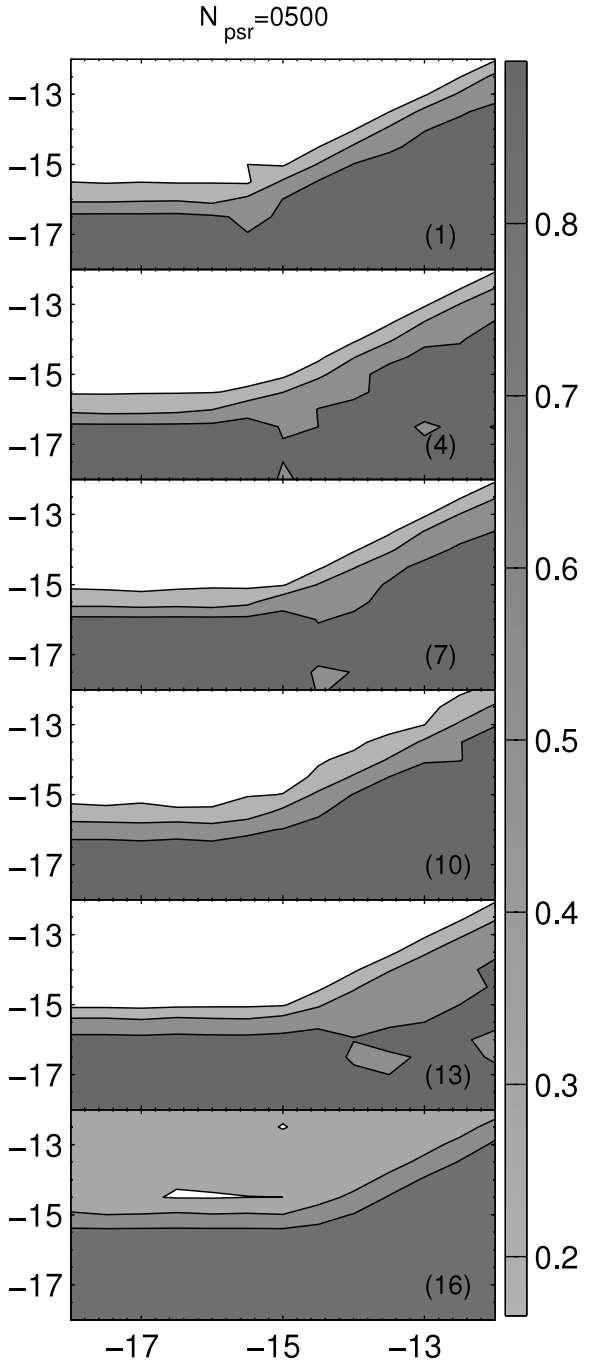

FIG. 8.—Same as Fig. 3, but for 500 pulsars and only for the shear mode.

where M is the number of pulsar pairs and $K(\gamma^P)$ depends on the four polarization "strengths" γ^P. In order to assure that each γ^P is positive, the cost function is set to its maximum value when any parameter is negative. The γ^P strengths are determined by minimizing the cost function using the improved downhill simplex method developed by Jeffrey et al. (1998).

We turn now to the question of detecting the non-Einsteinian modes in the presence of a background made up of Einsteinian GWs. Given a set of pulsars with a specified rms timing noise and specified power in the Einsteinian GW background, we calculate the minimum number of pulsars required to detect the non-Einsteinian modes. This is done using a standard Neyman-Pearson–style technique. Here, we only consider the case of a

background composed of Einsteinian GWs with one other alternative mode. The Neyman-Pearson false alarm rate is set at 0.001, and a Monte Carlo simulation is used to determine the detection threshold for the γ^P of interest. This is done by generating 5000 trial backgrounds that contain only the Einsteinian modes and determining the cumulative probability distribution for the γ^P of the non-Einsteinian mode. Once the detection threshold is determined, the false dismissal rate as a function of the power-law amplitude (the effective A_c) of that mode is determined from the simulations which now include the alternative mode. We take the astrophysically interesting ranges of amplitude A_c and index α to be those theoretically predicted for GR modes as presented in Jenet et al. (2005) and summarized in Table 2, taken from that reference.

Gray-scale plots of the false dismissal rate for different observing scenarios and GW background compositions are given in Figures 3–7, using 20, 40, 60, 100, and 300 pulsars, respectively. In these figures, the horizontal axis represents the base 10 logarithm of the characteristic strain spectrum of the Einsteinian GWs at a period of 1 yr. The vertical axis is the same but for the non-Einsteinian mode in question. For each plot, the exact wave mode and observing parameters are given in Table 3. For the shear mode, 300 pulsars are not enough to establish the 10% false dismissal rate, so shear mode results for 500 pulsars are given in Figure 8. In each of the plots, the contours become independent of the amplitude of the GR mode when the GR mode is small. This is expected since the dominant noise source becomes the pulsar timing noise for the case of a low-amplitude GR background. It can also be seen that the minimum detectable amplitude for the alternative mode is close to that of the GR mode when the GR signal is important, although for the longitudinal mode, the minimum detectable amplitude can be an order of magnitude smaller. These results show that in order to detect a non-GR mode in the presence of a GR mode with a 90% detection rate, one must use at least 40, 100, and 500 pulsars for the breathing, longitudinal, and shear modes, respectively.

5. CONCLUSION AND DISCUSSION

Precise pulsar timing observations allow one to measure the cross-correlation between the timing residuals of pulsar pairs and compare it with the cross-correlation theoretically predicted to result from the effect of GWs. In the case of an isotropic stochastic background of GWs, this correlation depends only on the angular separation θ separating the pair of pulsars. For GWs with Einsteinian polarization, the theoretical cross-correlation function $C(\theta)$ has a definitive shape. It has been shown here that when one allows for the additional four polarization modes of a general metric theory of gravity, the correlation function is a weighted sum of four possible curves, with each weight corresponding to the amplitude of each of the four distinct classes of GWs. Hence, a precise measurement of the angular correlation function can, in principle, determine the GW polarization properties of the GWs making up the stochastic background.

We investigated the possibility of detecting a stochastic background of GWs made up of each GW polarization class. If biweekly observations are made for five years with rms timing accuracy of 100 ns, then 60 pulsars are required for the longitudinal mode; 60 for the two spin-1 "shear" modes; and 40 for the spin-0 "breathing" mode. We confirmed the previous estimate in Jenet et al. (2005) that 40 pulsars are needed for the detection of the GR modes. As Figure 2 makes clear, whitening can greatly help to achieve improved detectability. Using whitening techniques, the number of pulsars needed drops to 30, 30, 20, and 20 for longitudinal, shear, breathing, and GR modes, respectively.

We have also investigated the possibility of discriminating between different polarization modes in the presence of a background of Einsteinian GWs. To determine the number of pulsars needed, Monte Carlo–style simulations were used to create a GW background composed of an Einsteinian mode and one non-Einsteinian mode. The probability of detecting the non-Einsteinian mode was determined as a function of the GW characteristic strain amplitudes. It was found that 40, 60, and 500 pulsars are needed to detect the breathing, longitudinal, and shear modes, respectively, in the presence of an Einsteinian mode. It was also found that the number of pulsars required is insensitive to the amplitude of the pulsar timing noise. As expected, the minimum detectable amplitude of each of the modes does depend on the timing noise level.

Previously, Jenet et al. (2005) used existing millisecond pulsar timing data to put upper limits on low-frequency GR GWs. With the results of the analysis in this paper, it is possible also to put limits on non-GR low-frequency GWs. A paper on these limits is in preparation (Lee et al. 2008, in preparation).

Of the several non-Einsteinian polarization modes, the longitudinal mode is of special interest for pulsar timing. As shown in Appendix A (see eq. [A37]), the amplitude of the induced timing residual for this mode is proportional to the distance from the pulsar to Earth, and the distances are several kiloparsecs for pulsars in the Galaxy. Thus, the response of the pulsar timing signal to longitudinal GWs is a few thousand times greater than the response to Einsteinian GWs. Extragalactic pulsars offer other interesting possibilities. If good timing accuracy (100 ns) can be achieved for such pulsars, they could be important tools for the study of longitudinal GW modes.

For all GW models and polarization modes, one element of pulsar timing is critical: a large sample of observed pulsars. In this regard, the future Square Kilometer Array will offer a unique opportunity to detect and characterize the stochastic GW background.

We gratefully acknowledge support by the National Science Foundation under grants AST 05-45837 and PHY 05-54367. We also thank the NASA Center for Gravitational Wave Astronomy at University of Texas at Brownsville. K. J. L. received travel support from NSFC (10521001, 10573002, 10778611, 10773016) and the Key Grant Project of the Chinese Ministry of Education (305001). Most of the Monte Carlo simulations were done on supercomputers at the Texas Advanced Computing Center (TACC).

APPENDIX A

ADDITIONAL CALCULATIONS

Some of the notation used in this paper is listed in Table 4.

TABLE 4
NOTATION

Symbol	Note
$h_{ab}(t)$	GW strain
$h_c^P(f)$	Characteristic strain for polarization P
Ω	Solid angle
$\mathbf{J}(f)$	Coherency matrix for GW
$C(\theta)$	Cross-correlation of pulsar timing residuals
P	Polarization index
f	GW frequency
ϵ_{ab}^P	Polarization tensor
$R(t)$	Timing residuals
$\hat{\boldsymbol{n}}$	Unit vector of pulsar position
$\hat{\boldsymbol{e}}_z$	Unit vector of GW's propagation direction

A1. STOCHASTIC GW BACKGROUND IN A GENERAL METRIC THEORY

In a general metric theory, the spatial part of the metric perturbation at given spacetime point $(t, \boldsymbol{r})$ can be written as the integral in equation (1),

$$h_{ab}(t,\boldsymbol{r}) = \sum_{P=+,\times,b,\mathrm{sn},\mathrm{se},l} \int_{-\infty}^{\infty} df \int d\Omega\, h^P(f,\hat{\boldsymbol{e}}_z) e^{2\pi i f\left(t-\boldsymbol{r}\cdot\hat{\boldsymbol{e}}_z/c\right)} \epsilon_{ab}^P(\hat{\boldsymbol{e}}_z), \tag{A1}$$

where the superscript P denotes the polarization state, Ω is the solid angle, $\hat{\boldsymbol{e}}_z$ is the unit vector in the direction of GW propagation, h^P is the amplitude of the GW with polarization state P, ϵ_{ab}^P is the polarization tensor for the polarization state P, and f is the GW frequency. The polarization tensors are best described in terms of the GW propagation vector $\hat{\boldsymbol{e}}_z$ and two other orthogonal unit vectors $\hat{\boldsymbol{e}}_x$ and $\hat{\boldsymbol{e}}_y$ transverse to $\hat{\boldsymbol{e}}_z$, as shown in Figure 9. In terms of these, the polarization tensors associated with a GW propagating along the $\hat{\boldsymbol{e}}_z$-direction are

$$\begin{aligned} \epsilon_{ab}^{+} &= \hat{\boldsymbol{e}}_{x,a}\hat{\boldsymbol{e}}_{x,b} - \hat{\boldsymbol{e}}_{y,a}\hat{\boldsymbol{e}}_{y,b}, \qquad \epsilon_{ab}^{\times} = \hat{\boldsymbol{e}}_{x,a}\hat{\boldsymbol{e}}_{y,b} + \hat{\boldsymbol{e}}_{y,a}\hat{\boldsymbol{e}}_{x,b}, \qquad \epsilon_{ab}^{b} = \hat{\boldsymbol{e}}_{x,a}\hat{\boldsymbol{e}}_{x,b} + \hat{\boldsymbol{e}}_{y,a}\hat{\boldsymbol{e}}_{y,b}, \\ \epsilon_{ab}^{\mathrm{sn}} &= \hat{\boldsymbol{e}}_{x,a}\hat{\boldsymbol{e}}_{z,b} + \hat{\boldsymbol{e}}_{z,a}\hat{\boldsymbol{e}}_{x,b}, \qquad \epsilon_{ab}^{\mathrm{se}} = \hat{\boldsymbol{e}}_{y,a}\hat{\boldsymbol{e}}_{z,b} + \hat{\boldsymbol{e}}_{z,a}\hat{\boldsymbol{e}}_{y,b}, \qquad \epsilon_{ab}^{l} = \hat{\boldsymbol{e}}_{z,a}\hat{\boldsymbol{e}}_{z,b}. \end{aligned} \tag{A2}$$

If the GW background is stationary and isotropic, the statistical properties of the GWs are described by $\mathbf{J}^{PP'}(f)$, a coherency matrix for GWs similar to the coherency matrix for electromagnetic waves (Born & Wolf 1999), and defined by

$$\left\langle h^P(f,\hat{\boldsymbol{e}}_z) h^{P'\star}\left(f',\hat{\boldsymbol{e}}_z'\right)\right\rangle = \frac{1}{4\pi}\delta(f-f')\delta\left(\hat{\boldsymbol{e}}_z-\hat{\boldsymbol{e}}_z'\right)\mathbf{J}^{PP'}(f). \tag{A3}$$

Here, $\star$ indicates the complex conjugate, and the delta function has the meaning

$$\int f(\hat{\boldsymbol{e}}_z)\delta(\hat{\boldsymbol{e}}_z-\hat{\boldsymbol{n}}_0)d\Omega = 4\pi f(\hat{\boldsymbol{n}}_0)$$

in which the Ω-integration varies the direction of $\hat{\boldsymbol{e}}_z$ over the 2-sphere. From equations (A1) and (A3) it follows that

$$\langle h_{ab}(t)h_{ab}(t)\rangle = \sum_P \int_0^{\infty} \eta(P)\mathbf{J}^{PP'}(f)df, \tag{A4}$$

where $\eta(P) \equiv 2^{PP}_{abab} = 4$, if $P = +, \times, b, \mathrm{sn}, \mathrm{se}$; and $\eta(P) = 2$, if $P = l$.

If one assumes that the background is not only stationary and isotropic, but also independently polarized (i.e., that $\mathbf{J}^{PP'} = \mathbf{0}$, if $P \neq P'$), then $\mathbf{J}^{PP'}(f)$ can be written as

$$\mathbf{J}^{PP'}(f) = \delta^{PP'}\frac{\left|h_c^P\right|^2(f)}{\eta(P)f}, \tag{A5}$$

so that

$$\langle h_{ab}(t)h_{ab}(t)\rangle = \sum_P \int_0^{\infty} \frac{\left|h_c^P\right|^2}{f}df. \tag{A6}$$

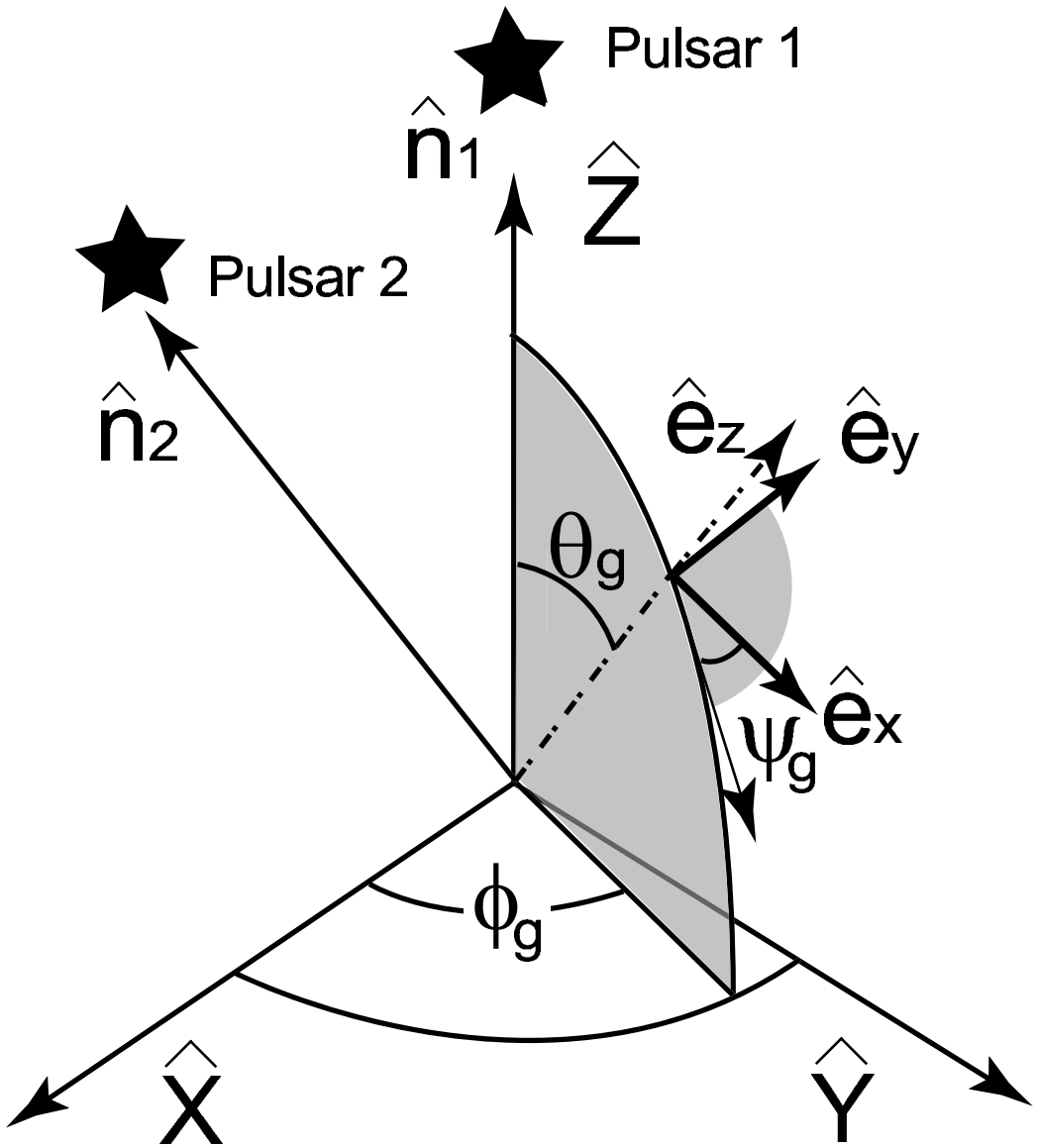

FIG. 9.—Geometric configuration of the coordinates and unit vectors used here. The $\hat{\boldsymbol{X}}$, $\hat{\boldsymbol{Y}}$, and $\hat{\boldsymbol{Z}}$ are the coordinate unit vectors, $\hat{\boldsymbol{e}}_z$ is the propagation direction of the GW, and $\hat{\boldsymbol{n}}_1$ and $\hat{\boldsymbol{n}}_2$ are unit vectors pointing to the pulsars.

A2. CORRELATION FUNCTION OF PULSAR TIMING RESIDUE

It follows from equation (A1) that

$$\int_0^T h_{ab}(t,\boldsymbol{r})dt = \sum_{P=+,\times,b,\mathrm{sn},\mathrm{se},l} \int_{-\infty}^{\infty} df \int d\Omega\, h^P(f,\hat{\boldsymbol{e}}_z)\epsilon^P_{ab}(\hat{\boldsymbol{e}}_z)e^{-2\pi fi\boldsymbol{r}\cdot\hat{\boldsymbol{e}}_z/c}\frac{e^{2\pi fiT}-1}{2f\pi}. \tag{A7}$$

From this and equations (2) and (3), the pulsar timing residual is found to be[3]

$$R(t) = \frac{1}{2}\sum_{P=+,\times,b,\mathrm{sn},\mathrm{se},l} \int_{-\infty}^{\infty} df \int d\Omega\, h^P(f,\hat{\boldsymbol{e}}_z)\epsilon^P_{ab}(\hat{\boldsymbol{e}}_z)\hat{\boldsymbol{n}}^i\hat{\boldsymbol{n}}^{\,j}B, \tag{A8}$$

$$B = \frac{\left(e^{2\pi fit}-1\right)\left(1-e^{-2\pi ifD\left(1+\hat{\boldsymbol{n}}\cdot\hat{\boldsymbol{e}}_z\right)/c}\right)}{2\pi fi(1+\hat{\boldsymbol{e}}_z\cdot\hat{\boldsymbol{n}})}, \tag{A9}$$

where $D_i \equiv |\boldsymbol{r}_{\mathrm{pul},i}|$ is the distance to pulsar i.

[3] It should be noted that in one specific reference frame $h_{ab,00} = -2R_{a0b0}$ (Thorne 1983), i.e., the metric perturbation can be expressed in terms of Riemann components. Thus, in principle all calculations here involving h_{ab} can be replaced by calculations involving Riemann components. Since the Riemann tensor is gauge-invariant, the final results we derive here should be regarded as gauge-invariant, although the calculation is performed using gauge-dependent metric perturbations h_{ab}.

The angular separation θ between two pulsars is given by $\theta = \arccos(\hat{\boldsymbol{n}}_i \cdot \hat{\boldsymbol{n}}_j)$, where $\hat{\boldsymbol{n}}_i$ and $\hat{\boldsymbol{n}}_j$ are the unit position vectors for the two pulsars. The cross-correlation function $C(\theta)$ of the ith and the jth pulsar's timing residual is denoted as $C(\theta) = \langle R_i(t) R_j(t) \rangle$. To compute this we multiply the expressions in equations (A8) and (A9) by the equivalent expression for pulsar j (formally using the complex conjugate of this real expression). With the delta functions in equation (A3) we can immediately do the integrals over one frequency and one solid angle.

The ensemble average over the stochastic GW background can be replaced by an average over a long time. From the "B" factors, of equation (A9), for pulsars i and j, we get

$$\begin{aligned} PT &\equiv \frac{1}{4} \lim_{T\to\infty} \frac{1}{T} \int_0^T dT \left[\left(e^{2\pi f i t} - 1\right) \left(1 - e^{-2\pi i f D_i \left(1 + \hat{\boldsymbol{n}}_i \cdot \hat{\boldsymbol{e}}_z\right)/c}\right) \right] \left[\left(e^{2\pi f i t} - 1\right) \left(1 - e^{-2\pi i f D_j \left(1 + \hat{\boldsymbol{n}}_j \cdot \hat{\boldsymbol{e}}_z\right)/c}\right) \right]^{\star} \\ &= \left\{ 1 - \cos\left(2\pi f \Delta_i\right) - \cos\left(2\pi f \Delta_j\right) + \cos\left[2\pi f \left(\Delta_i - \Delta_j\right)\right] \right\} / 2, \end{aligned} \tag{A10}$$

where $\Delta_i = (1 + \hat{\boldsymbol{n}}_i \cdot \hat{\boldsymbol{e}}_z) D_i / c$. In terms of the PT factor, the theoretical cross-correlation function can be written

$$C(\theta) = \sum_P C^P(\theta), \tag{A11}$$

$$C^P(\theta) = \left\langle \frac{1}{4\pi} \int_0^\infty \frac{\left|h_c^P\right|^2(f)}{\eta 4\pi^2 f^3} df \int d\Omega \frac{\hat{\boldsymbol{n}}_i \cdot {}^P \cdot \hat{\boldsymbol{n}}_i}{1 + \hat{\boldsymbol{n}}_i \cdot \hat{\boldsymbol{e}}_z} \frac{\hat{\boldsymbol{n}}_j \cdot {}^P \cdot \hat{\boldsymbol{n}}_j}{1 + \hat{\boldsymbol{n}}_j \cdot \hat{\boldsymbol{e}}_z} PT \right\rangle. \tag{A12}$$

This result assumes that the GW background is independently polarized. If the polarization is *not* independent (i.e., $\mathbf{J}^{PP'} \neq 0$, for $P \neq P'$), the cross-correlation functions $C^P(\theta)$ will have contributions only from the correlation between the longitudinal and the breathing modes, i.e., only from $\mathbf{J}^{bl}$. Furthermore, it can be shown that $C^P(\theta)$ induced by $\mathbf{J}^{bl}$ has exactly the same form as the $C^P(\theta)$ induced by the shear modes.

We now consider the way in which polarization properties enter into the evaluation of $C^P(\theta)$. In Figure 9, the components of $\hat{\boldsymbol{e}}_z$ in the $\hat{\boldsymbol{X}}^a = (\hat{\boldsymbol{X}}, \hat{\boldsymbol{Y}}, \hat{\boldsymbol{Z}})$ frame can be seen to be $\left[\sin(\theta_g)\cos(\phi_g), \sin(\theta_g)\sin(\phi_g), \cos(\theta_g)\right]$, where the θ_g and ϕ_g are respectively the polar angle and azimuthal angle of the GW propagation vector. To proceed, we need the components of the polarization tensors in the $\hat{\boldsymbol{X}}^a$ frame. The transformation from the components $\epsilon_{0,cd}$ given in the GW frame $\hat{\boldsymbol{e}}_b = (\hat{\boldsymbol{e}}_x, \hat{\boldsymbol{e}}_y, \hat{\boldsymbol{e}}_z)$, of equation (A2), is made with $\epsilon^P_{ab} = T_{ca} T_{db} \epsilon^P_{0,cd}$, where $T_{ca} = \hat{\boldsymbol{e}}_c \cdot \hat{\boldsymbol{X}}_a$ has components

$$\begin{pmatrix} \cos\theta_g \cos\phi_g \cos\psi_g - \sin\phi_g \sin\psi_g & \cos\theta_g \cos\psi_g \sin\phi_g + \cos\phi_g \sin\psi_g & -\cos\psi_g \sin\theta_g \\ -\cos\psi_g \sin\phi_g - \cos\theta_g \cos\phi_g \sin\psi_g & \cos\phi_g \cos\psi_g - \cos\theta_g \sin\phi_g \sin\psi_g & \sin\theta_g \sin\psi_g \\ \cos\phi_g \sin\theta_g & \sin\theta_g \sin\phi_g & \cos\theta_g \end{pmatrix}. \tag{A13}$$

Since the GW background is isotropic, with no loss of generality one can choose $\hat{\boldsymbol{n}}_i \equiv \hat{\boldsymbol{n}}_1 = (0, 0, 1)$ and $\hat{\boldsymbol{n}}_j \equiv \hat{\boldsymbol{n}}_2 = [\sin(\theta), 0, \cos(\theta)]$ so that

$$1 + \hat{\boldsymbol{n}}_1 \cdot \hat{\boldsymbol{e}}_z = \cos\theta_g + 1, \qquad 1 + \hat{\boldsymbol{n}}_2 \cdot \hat{\boldsymbol{e}}_z = \cos\theta\cos\theta_g + \cos\phi_g \sin\theta \sin\theta_g + 1,$$

and PT takes the relatively simple form

$$\begin{aligned} PT = 1/2 &- 1/2 \cos\left[2\pi f c^{-1} D_1 \left(1 + \cos\theta_g\right)\right] - 1/2 \cos\left[2\pi f c^{-1} D_2 \left(1 + \sin\theta\cos\phi_g \sin\theta_g + \cos\theta\cos\theta_g\right)\right] \\ &+ 1/2 \cos\left\{2\pi f c^{-1} \left[D_1 \left(1 + \cos\theta_g\right) - D_2 \left(1 + \sin\theta\cos\phi_g \sin\theta_g + \cos\theta\cos\theta_g\right)\right]\right\}. \end{aligned} \tag{A14}$$

With the transformation in equation (A13), it is straightforward to evaluate the polarization factors in equation (A12),

$$\hat{\boldsymbol{n}}_1 \cdot \boldsymbol{\epsilon}^+ \cdot \hat{\boldsymbol{n}}_1 = \cos(2\psi_g) \sin^2\theta_g, \tag{A15}$$

$$\begin{aligned} \hat{\boldsymbol{n}}_2 \cdot \boldsymbol{\epsilon}^+ \cdot \hat{\boldsymbol{n}}_2 = {} & \cos(2\psi_g) \left[\left(\cos\theta_g \cos\phi_g \sin\theta - \cos\theta \sin\theta_g\right)^2 - \sin^2\theta \sin^2\phi_g \right] \\ & - \left[2\cos\theta_g \cos\phi_g \sin^2\theta - \sin(2\theta)\sin\theta_g\right] \sin\phi_g \sin(2\psi_g), \end{aligned} \tag{A16}$$

$$\hat{\boldsymbol{n}}_1 \cdot \boldsymbol{\epsilon}^\times \cdot \hat{\boldsymbol{n}}_1 = -2\cos\psi_g \sin^2\theta_g \sin\psi_g, \tag{A17}$$

$$\begin{aligned} \hat{\boldsymbol{n}}_2 \cdot \boldsymbol{\epsilon}^\times \cdot \hat{\boldsymbol{n}}_2 = {} & \cos\theta_g \sin^2\theta \sin(2\phi_g) \sin^2\psi_g - 2\cos\psi_g \left[\left(\cos\theta_g \cos\phi_g \sin\theta - \cos\theta \sin\theta_g\right)^2 - \sin^2(\theta)\sin^2(\phi_g) \right] \sin(\psi_g) \\ & + 2\sin(\theta) \left[\cos(\theta)\cos(2\psi_g)\sin(\theta_g) - \cos(\theta_g)\cos(\phi_g)\cos^2(\psi_g)\sin(\theta) \right] \sin(\phi_g), \end{aligned} \tag{A18}$$

$$\hat{\boldsymbol{n}}_1 \cdot \boldsymbol{\epsilon}^{\mathrm{sn}} \cdot \hat{\boldsymbol{n}}_1 = -2\cos\theta_g \cos\psi_g \sin\theta_g, \tag{A19}$$

$$\hat{\boldsymbol{n}}_2 \cdot \boldsymbol{\epsilon}^{\mathrm{sn}} \cdot \hat{\boldsymbol{n}}_2 = -2\left(\cos\theta\cos\theta_g + \cos\phi_g \sin\theta \sin\theta_g\right)\left(-\cos\theta_g \cos\phi_g \cos\psi_g \sin\theta + \sin\phi_g \sin\psi_g \sin\theta + \cos\theta\cos\psi_g \sin\theta_g\right), \tag{A20}$$

$$\hat{\boldsymbol{n}}_1 \cdot \boldsymbol{\epsilon}^{\rm se} \cdot \hat{\boldsymbol{n}}_1 = \sin(2\theta_g)\sin\psi_g, \tag{A21}$$

$$\hat{\boldsymbol{n}}_2 \cdot \boldsymbol{\epsilon}^{\rm se} \cdot \hat{\boldsymbol{n}}_2 = 2\big(\cos\theta\cos\theta_g + \cos\phi_g \sin\theta\sin\theta_g\big)\big[\big(\cos\theta\sin\theta_g - \cos\theta_g\cos\phi_g\sin\theta\big)\sin\psi_g - \cos\psi_g\sin\theta\sin\phi_g\big], \tag{A22}$$

$$\hat{\boldsymbol{n}}_1 \cdot \boldsymbol{\epsilon}^{b} \cdot \hat{\boldsymbol{n}}_1 = \sin^2\theta_g, \tag{A23}$$

$$\hat{\boldsymbol{n}}_2 \cdot \boldsymbol{\epsilon}^{b} \cdot \hat{\boldsymbol{n}}_2 = \big(\cos\theta_g\cos\phi_g\sin\theta - \cos\theta\sin\theta_g\big)^2 + \sin^2\theta\sin^2\phi_g, \tag{A24}$$

$$\hat{\boldsymbol{n}}_1 \cdot \boldsymbol{\epsilon}^{l} \cdot \hat{\boldsymbol{n}}_1 = \cos^2\theta_g, \tag{A25}$$

$$\hat{\boldsymbol{n}}_1 \cdot \boldsymbol{\epsilon}^{l} \cdot \hat{\boldsymbol{n}}_1 = \big(\cos\theta\cos\theta_g + \cos\phi_g\sin\theta\sin\theta_g\big)^2. \tag{A26}$$

The GW polarization modes are divided into two classes: the three transverse polarizations $+$, $\times$, and b; and the three polarizations sn, se, and l that are not purely transverse. We first consider the transverse modes, and we start with the polarization $+$. The ensemble average involves an average over ψ_g, and with this averaging we have

$$F_+(\theta,\theta_g,\phi_g) \equiv \langle(\hat{\boldsymbol{n}}_1\cdot\boldsymbol{\epsilon}^+\cdot\hat{\boldsymbol{n}}_1)(\hat{\boldsymbol{n}}_2\cdot\boldsymbol{\epsilon}^+\cdot\hat{\boldsymbol{n}}_2)\rangle_{\psi_g} = \frac{1}{2}\sin^2\theta_g\Big[\big(\cos\theta_g\cos\phi_g\sin\theta - \cos\theta\sin\theta_g\big)^2 - \sin^2\theta\sin^2\phi_g\Big]. \tag{A27}$$

The angular averaging in equation (A12) then involves

$$\int_0^{2\pi} d\phi_g \int_0^{\pi} \sin\theta_g\, d\theta_g \frac{F_+(\theta,\theta_g,\phi_g)PT}{\big(\cos\theta_g+1\big)\big(\cos\theta\cos\theta_g + \cos\phi_g\sin\theta\sin\theta_g + 1\big)}. \tag{A28}$$

In the numerator, the cosine terms in PT contain a factor $fc^{-1}D$ that is the ratio of the pulsar distance to the GW wavelength, a factor of order $D/\lambda \sim 10^3 \gg 1$. The integral of the terms with these rapid oscillations can be evaluated using the method of stationary phase. The result will contain powers of the small factor λ/D and will be negligible. We can therefore evaluate the angular integrals using $PT = 1/2$ if $\theta \neq 0$. In the case $\theta = 0$, that is, the autocorrelation $C^P(0)$, we have $\Delta_0 = \Delta_1$, so the last term in equation (A10) is not oscillatory, and for the nonoscillatory part of PT, we have 1 rather than 1/2. For $\theta \neq 0$, the result of the integral in equation (A28) is

$$(\pi/3)(\cos\theta - 6(\cos\theta - 1)\{\log[(1-\cos\theta)/2] + 3)\}). \tag{A29}$$

At $\theta = 0$ the value is doubled, since in this case, we have $PT = 1$ rather than $PT = 1/2$. We write the result as $(16\pi/3)\zeta^{\rm GR}(\theta)$ with

$$\zeta^{\rm GR}(\theta) = \frac{3(1-\cos\theta)}{4}\log\left(\frac{1-\cos\theta}{2}\right) + \frac{1}{2} - \frac{1-\cos\theta}{8} + \frac{\delta(\theta)}{2}, \tag{A30}$$

in which $\delta(\theta) = 1$ if $\theta = 0$ and vanishes for $\theta \neq 0$. Although we have specified the $+$ polarization, the result after ensemble averaging (or averaging over ψ_g) must be the same for the $\times$ polarization. The integral in equation (A12) then gives us the following as the high-frequency (small λ/D) limit for either GR mode (Hellings & Downs 1983),

$$C^{+,\times}(\theta) = \zeta^{\rm GR}(\theta)\int_0^{\infty}\frac{\big|h_c^{+,\times}\big|^2}{24\pi^2 f^3}df. \tag{A31}$$

The pattern of calculation for the breathing mode is similar to that for the GR modes. The angular factor F_+ is replaced by

$$F_b(\theta,\theta_g,\phi_g) \equiv \big(\hat{\boldsymbol{n}}_1\cdot\boldsymbol{\epsilon}^b\cdot\hat{\boldsymbol{n}}_1\big)\big(\hat{\boldsymbol{n}}_2\cdot\boldsymbol{\epsilon}^b\cdot\hat{\boldsymbol{n}}_2\big) = \sin^2\theta_g\Big[\big(\cos\theta_g\cos\phi_g\sin\theta - \cos\theta\sin\theta_g\big)^2 + \sin^2\theta\sin^2\phi_g\Big]. \tag{A32}$$

As in the GR case, we can ignore the rapidly oscillating terms in PT and can use $PT = 1/2$ for $\theta \neq 0$ and $PT = 1$ for $\theta = 0$. The result of the angular integration, in the short-wavelength approximation, is

$$\int_0^{2\pi}\int_0^{\pi}\frac{\sin\theta_g\, d\theta_g\, d\phi_g\, F_b(\theta,\theta_g,\phi_g)PT}{\big(\cos\theta_g+1\big)\big(\cos\theta\cos\theta_g + \cos\phi_g\sin\theta\sin\theta_g + 1\big)} = \frac{2\pi}{3}[\cos\theta + 3 + 4\delta(\theta)]. \tag{A33}$$

To put this in a form analogous to that of equation (A31), we define

$$\zeta^b(\theta) \equiv \frac{1}{8}[\cos\theta + 3 + 4\delta(\theta)], \tag{A34}$$

and we write the final short-wavelength approximation as

$$C^b(\theta) = \zeta^b(\theta)\int_0^{\infty}\frac{\big|h_c^b\big|^2}{12\pi^2 f^3}df. \tag{A35}$$

In the geometric integrals of equations (A28) and (A33), the factors in the denominator, $1 + \hat{\boldsymbol{n}}_1 \cdot \hat{\boldsymbol{e}}_z$ and $1 + \hat{\boldsymbol{n}}_2 \cdot \hat{\boldsymbol{e}}_z$, vanish when the propagation direction of the GW corresponds to the direction of propagation of the pulsar signal. For the purely transverse modes, the polarization projections $(\hat{\boldsymbol{n}}_1 \cdot \boldsymbol{\epsilon}^P \cdot \hat{\boldsymbol{n}}_1)(\hat{\boldsymbol{n}}_2 \cdot \boldsymbol{\epsilon}^P \cdot \hat{\boldsymbol{n}}_2)$ in the numerator vanish also for these alignments, and the integrals are not dominated by contributions near the values of θ_g, ϕ_g corresponding to alignment. For the polarizations that are not purely transverse, the longitudinal and shear modes, this is not the case. The polarization projections do not vanish strongly enough to cancel the vanishing of the denominator. The behavior of PT near alignment must therefore be considered, and the result is that the geometric integral becomes dependent on the frequency and the distance to the pulsars.

We start the consideration of the modes that are not purely transverse with the longitudinal case. To simplify, we introduce the notation $\Phi_i = 2\pi f c^{-1} D_i$ and $N_i = 1 + \hat{\boldsymbol{n}}_i \cdot \hat{\boldsymbol{e}}_z$ for $i = 1, 2$. The autocorrelation, corresponding to $\theta = 0$ in equations (A14)–(A26) and to $\Phi_1 = \Phi_2 \equiv \Phi$ and $N_1 = N_2 = 1 + \cos\theta_g$, gives us the integral

$$\int_0^{2\pi} d\phi_g \int_{-1}^{1} d\cos\theta_g \frac{F_l(\theta, \theta_g, \phi_g) PT}{\left(\cos\theta_g + 1\right)^2} = 2\pi \int_0^2 dN \frac{(1 - \cos N\Phi)(1 - N)^4}{N^2} = 2\pi\left[\frac{\pi}{2}\Phi - 4\log\Phi + O\left(\Phi^0\right)\right] \approx \pi^2\Phi, \tag{A36}$$

where the large Φ approximation is made since the number of GW wavelengths in the pulsar distance is on the order of 10^3. With this result we have

$$C^l(0) = \int_0^\infty \frac{\left|h_c^{+,\times}\right|^2}{32\pi^3 f^3} \pi^2 \frac{2\pi f D}{c} df. \tag{A37}$$

For $\theta \neq 0$ a closed-form answer analogous to equation (A37) is not possible, but it is not difficult to see the way in which the values of Φ_0 and Φ_1 influence the result. We start by writing PT as

$$PT = 2\sin^2(N_1\Phi_1/2)\sin^2(N_2\Phi_2/2) + (1/2)\sin N_1\Phi_1 \sin N_2\Phi_2 \tag{A38}$$

and the geometric integral as

$$\int_0^{2\pi} d\phi_g \int_{-1}^{1} d\cos\theta_g \frac{F_l(\theta, \theta_g, \phi_g) PT}{N_1 N_2} = \int_0^{2\pi} d\phi_g \int_0^2 dN_1 \frac{(N_1 - 1)(N_2 - 1)}{N_1 N_2} PT. \tag{A39}$$

In the limit of large Φ_i, the integral is dominated by the contributions near $\Phi_i = 0$. By the symmetry in the integral, the contributions near $\Phi_1 = 0$ and $\Phi_2 = 0$ must be the same, so we focus on the former. Since PT vanishes at $\Phi_1 = 0$, the integrand is bounded, but due to the factor $\sin^2(N_1\Phi_1/2)/N_1$, the integral has a logarithmic dependence on Φ_1; in fact,

$$\int_0^{2\pi} d\phi_g \int_0^2 dN_0 \frac{\sin^2(N_0\Phi_0/2)}{N_0} = \pi[\gamma + \log 2\Phi_0 - \mathrm{Ci}(2\Phi_0)] \approx \pi(\gamma + \log 2\Phi_0), \tag{A40}$$

where γ is the Euler constant and where $\mathrm{Ci}(2\Phi_0)$ is the cosine integral function of $2\Phi_0$ and is negligibly small for large Φ_0. The omitted, slowly varying factor $(N_2 - 1)/N_2$ can be evaluated at $\theta = \pi$. The rapidly varying factor $\sin^2(N_2\Phi_2/2)$ has a more complicated effect, since it varies rapidly with N_1. Nevertheless, the resulting integral is still logarithmic in Φ_0 (and of course in Φ_1). The calculation of cross-correlation function $C^{\mathrm{sn,se}}(\theta)$ will therefore be different for different values of the Earth-pulsar distances D_1, D_2 and for different GW spectra. For this reason, $C^{\mathrm{sn,se}}(\theta)$ must be computed by the Monte Carlo technique described in § 2.

For the shear modes the details are different in a significant way. At $\theta = 0$ the ψ_g average of the sn or se polarization projection is

$$F_{\mathrm{sh}}(\theta, \theta_g, \phi_g) = \left\langle (\hat{\boldsymbol{n}}_1 \cdot \boldsymbol{\epsilon}^{\mathrm{sn}} \cdot \hat{\boldsymbol{n}}_1)^2 \right\rangle_{\psi_g} = \left\langle (\hat{\boldsymbol{n}}_1 \cdot \boldsymbol{\epsilon}^{\mathrm{se}} \cdot \hat{\boldsymbol{n}}_1)^2 \right\rangle_{\psi_g} = 2\cos^2\theta_g \sin^2\theta_g. \tag{A41}$$

With the same form of PT as in equation (A36), the geometric integral then becomes

$$\begin{aligned} \int_0^{2\pi} d\phi_g \int_0^{\pi} \sin\theta_g\, d\theta_g \frac{F_{\mathrm{sh}}}{(1 + \cos\theta_g)^2} PT &= 4\pi \int_0^2 dN \frac{(N - 1)^2(2 - N)}{N}(1 - \cos N\Phi) \\ &= 4\pi\left[2\log(2\Phi) - \frac{14}{3} + 2\gamma - 2\mathrm{Ci}(2\Phi) + O\left(\frac{1}{\Phi}\right)\right], \end{aligned} \tag{A42}$$

and hence,

$$C^{\mathrm{sn,se}}(0) = 4\pi \int_0^\infty \frac{\left|h_c^{+,\times}\right|^2}{24\pi f^3}\left[2\log\left(\frac{4\pi f D}{c}\right) - \frac{14}{3} + 2\gamma - 2\mathrm{Ci}\left(\frac{4\pi f D}{c}\right) + O\left(\frac{c}{fD}\right)\right] df. \tag{A43}$$

If θ is not small, the denominator only has a single factor of N and F_{sh} has a single factor of $\sin\theta_g$, which is of order $N^{1/2}$ near $N = 0$. Thus, without the PT factor the integrand is of order $1/N^{1/2}$ and is integrable. We can therefore ignore the rapidly varying terms and

take PT simply to be 1/2. (This has been confirmed with Monte Carlo simulations.) With $PT = 1/2$, the integral for the shear cross-correlation can be done in closed form,

$$\int_0^{2\pi}\int_0^{\pi}\frac{d\phi_g \sin\theta_g\, d\theta_g\, F_{\rm sh}}{(1+\cos\theta_g)(1+\cos\theta_g\cos\theta+\cos\phi_g\sin\theta_g\sin\theta)}PT$$
$$= 4\pi\left[-1-\frac{4\cos\theta}{3}+\log\left(\frac{2}{1-\cos\theta}\right)\right]$$
$$\equiv \frac{8\pi}{3}\zeta^{\rm sh}(\theta), \tag{A44}$$

so that

$$C^{\rm sh}(\theta) = \zeta^{\rm sh}(\theta)\int_0^{\infty}\frac{\left|h_c^{\rm sh}\right|^2}{24\pi^2 f^3}df. \tag{A45}$$

This result only applies if the singularities at N_1 and at N_2 are well separated. The angular separation must be large enough so that PT has many oscillations as the direction of propagation of the GW $\hat{\boldsymbol{e}}_z$ moves from the $\hat{\boldsymbol{n}}_1$-direction to that of $\hat{\boldsymbol{n}}_2$ in Figure 9. This will be the case if $\Phi\theta \gg 1$, where Φ is the typical size of Φ_1 or Φ_2. This is also the condition for the cross-correlation angular integral in equation (A44) to be less than the autocorrelation in equation (A43) (in the limit of large Φ). To avoid dealing with the distinctions among the several regimes (autocorrelation, small angle, big angle) of the shear correlation, we have chosen to do all shear computations via the Monte Carlo technique.

REFERENCES

Born, M., & Wolf, E., eds. 1999, Principles of Optics: Electromagnetic Theory of Propagation, Interference and Diffraction of Light (Cambridge: Cambridge Univ. Press)
Detweiler, S. 1979, ApJ, 234, 1100
Eardley, D. M., Lee, D. L., & Lightman, A. P. 1973, Phys. Rev. D, 8, 3308
Enoki, M., Inoue, K. T., Nagashima, M., & Sugiyama, N. 2004, ApJ, 615, 19
Estabrook, F. B., & Wahlquist, H. D. 1975, Gen. Relativ. Gravitation, 6, 439
Grishchuk, L. P. 2005, Phys. Uspekhi, 48, 1235
Hellings, R. W., & Downs, G. S. 1983, ApJ, 265, L39
Jaffe, A. H., & Backer, D. C. 2003, ApJ, 583, 616
Jeffrey, C. L., James, A. R., Margaret, H. W., & Paul, E. W. 1998, SIAM J. Optimization, 9, 112
Jenet, F. A., Creighton, T., & Price, R. H. 2008, in preparation
Jenet, F. A., Hobbs, G. B., Lee, K. J., & Manchester, R. N. 2005, ApJ, 625, L123
Lee, K. J., Jenet, F. A., Price, R. H., Manchester, R. N., & Hobbs, G. B. 2008, in preparation
Maggiore, M. 2000, Phys. Rep., 331, 283
Sanders, R. H., & McGaugh, S. S. 2002, ARA&A, 40, 263
Sazhin, M. V. 1978, Soviet Astron., 22, 36
Thorne, K. S. 1983, in Gravitational Radiation, ed. N. Deruelle & T. Piran (Amsterdam: North-Holland), 1
Will, C. 2006, Living Rev. Relativ., 9, 3
Wyithe, J. S. B., & Loeb, A. 2003, ApJ, 590, 691